Climate Dynamics
https://doi.org/10.1007/s00382-020-05252-z

The fidelity of a regional coupled model in capturing the relationship between intraseasonal variability and the onset/demise of the Indian summer monsoon

Nirupam Karmakar[1] · **Vasubandhu Misra**[1,2,3]

Received: 17 December 2019 / Accepted: 15 April 2020

Abstract
Onset and demise of the Indian summer monsoon (ISM) and intraseasonal variability (ISV) embedded within the ISM are dominant climatological phenomena observed over the Indian region. In this study, a quantitative relationship between these two phenomena is assessed and the performance of a regional coupled model in simulating the relationship in the ISM is examined. An objective definition of the local onset and demise of the ISM is used based on more than a century-long India Meteorological Department rain-gauge observation and 10-year-long model simulated precipitation. Two distinct modes of intraseasonal oscillations (ISOs), northwestward propagating 10–20-day periodic high-frequency ISO and northward moving 20–70-day periodic low-frequency ISOs are extracted using Multichannel Singular Spectrum Analysis (MSSA). It is found that nearly 60% of the local onset of the ISM occurs during the positive developing phases of the ISO; whereas, a similar fraction of local demise occurs during positive decaying phases of the ISO across almost entire India. Essentially, the phase-locking of two ISOs creates the most conducive environment for onset or demise of the ISM to occur. In this study we found that the model not only captures the overall structure of the ISO modes, but also simulates the observed distribution of the onset and demise dates of ISM in different ISO phases. The diagnostics described here, with the ability of the model to produce the observed phenomena, provide an essential tool to improve our understanding of the monsoon system and its predictability.

Keywords Indian monsoon · Intraseasonal oscillation · Onset and demise of Indian Monsoon · Regional coupled model

1 Introduction

The Indian summer monsoon (ISM) possesses a unique seasonal cycle that can be regarded as one of the most prominent phenomena in the tropical climate. Apart from this strong seasonal cycle, the ISM exhibits variability in different space and time scales (Webster et al. 1998; Gadgil 2003). The basic system that governs the ISM and its variability is considered to be the Intertropical Convergence Zone (ITCZ) or the equatorial trough (Gadgil 2003). Northward shift of the ITCZ during the boreal summer sets the premise for the onset of the ISM. Given its severe socioeconomic and agricultural impact (Gadgil and Gadgil 2006; Giné et al. 2008), characterization of the variability in onset and demise events of the ISM has been a topic of rigorous investigative studies. Many studies documented a significant interannual variability in the observed date of onset of the ISM (Joseph et al. 1994; Wang and LinHo 2002; Misra et al. 2017b). The investigation of this variability largely depends upon how onset

Electronic supplementary material The online version of this article (https://doi.org/10.1007/s00382-020-05252-z) contains supplementary material, which is available to authorized users.

✉ Nirupam Karmakar
nirupam.ju@gmail.com; nkarmakar@fsu.edu

Vasubandhu Misra
vmisra@fsu.edu

[1] Earth, Ocean and Atmospheric Science Department, Florida State University, Tallahassee, FL 32306, USA

[2] Center for Ocean-Atmospheric Prediction Studies, Florida State University, Tallahassee, FL, USA

[3] Florida Climate Institute, Florida State University, Tallahassee, FL, USA

Published online: 07 May 2020

and demise of the ISM are defined. Some studies use rainfall as a measure to define these events (Ananthakrishnan et al. 1967; Sperber and Annamalai 2014; Noska and Misra 2016), some use circulation patterns over the Indian region (Webster and Yang 1992; Wang et al. 2009a), while others use land-ocean temperature contrast (Yanai et al. 1992; Zhou and Murtugudde 2014). Most of the definitions are based on defining a single index for onset/demise for the entire Indian domain, usually obtained through area averaging over a critical location. As an example, monsoon onset over Kerala is a widely-used index to determine monsoon onset over India (Ananthakrishnan et al. 1967; Joseph et al. 2006). However, a single index definition of onset/demise of the ISM could restrict understanding of the advance or evolution of the ISM. The monsoon onset over Kerala is not strongly coupled with the onset over other regions across India (Bansod et al. 1991). Therefore, onset based on one area average index only provides an indication whether the entire system has moved up to a desired region in an averaged sense. Conversely, a local definition, that defines onset/demise at the most granular scale possible would provide more insight into the progression of the monsoon isochrones. A few studies (Sperber and Annamalai 2014; Moron and Robertson 2014; Misra et al. 2017a; Karmakar and Misra 2019) have developed a regional or local definition for onset and demise of the ISM based on rainfall datasets.

While many argue that the single index definitions of onset of the ISM is legitimate based on the fact that the onset of the All-India Rainfall (AIR) is highly related to the large-scale changes in the ocean and atmospheric circulation and land-sea thermal contrast, these definitions do not provide information at the local or regional scale because of area averaging. In a country like India where livelihood largely depends on rain-fed agriculture, onset and rainfall prediction at the local scale is of paramount importance. Therefore, in this study we use a local definition of onset and demise of the ISM as defined in Misra et al. (2017a). The method described there is not only adaptive to any given spatial resolution of the rainfall dataset, but also tends to avoid false onsets and demise as it is anchored to the climatological evolution of the AIR.

Apart from the strong seasonal cycle of rainfall, the ISM also exhibits dominant intraseasonally varying patterns, that are strongly associated with intraseasonal oscillations (ISOs) (Sikka and Gadgil 1980; Yasunari 1980; Gadgil 2003; Goswami and Ajaya Mohan 2001; Krishnamurthy and Shukla 2007; Karmakar et al. 2017b). ISOs are mainly held responsible for modulating the active-break cycle over any particular region. Many studies suggest that there are two types of space-time scale variations associated with ISOs: (1) a low-frequency ISO (LF-ISO) exhibiting a periodicity between roughly 20–70 days (Sikka and Gadgil 1980; Yasunari 1980), and (2) a high-frequency ISO (HF-ISO) showing a variability of nearly 10–20 days (Krishnamurti and Bhalme 1976; Chen and Chen 1993; Krishnamurthy and Shukla 2007; Lee et al. 2013; Karmakar et al. 2017b). The 20–70 day periodic ISO is characterized by northward propagation of convection from the equatorial Indian Ocean to the foothills of the Himalayas; whereas, the high-frequency ISO shows a dominant north-westward propagation from the Bay of Bengal towards central and northwestern India. These two modes highly modulate the rainfall amount over the central Indian region, which is also the region most agriculturally vulnerable to seasonal and subseasonal rainfall anomalies (Krishnamurti et al. 1985; Karmakar et al. 2017b).

Onset over Myanmar preceedes Indian monsoon onset by about a month and monsoon onset over Kerala happens from the passage of a second wave of the LF-ISO (Krishnamurti et al. 2012). However, it is suggested that the onset of the ISM over Kerala and Western Ghats is linked with the first strong LF-ISO event of the year (Lau and Yang 1996; Zhou and Murtugudde 2014). Moreover, the retreat of the monsoon isochrone related to the demise of the ISM is not exactly the mirror image of the movement of the onset isochrone (Gadgil 2003). These make the relationship between ISO and onset/demise a complex phenomena.

Although our understanding of the ISOs has increased significantly in the past few decades, the state-of-the-art models are still limited by their simulation of the basic structure of monsoon intraseasonal variability (ISV) (Lin et al. 2008; Sabeerali et al. 2013). In spite of many improvements made between phase 3 of the Coupled Model Intercomparison Project (CMIP) to its phase 5 in terms of simulating the mean monsoon and subseasonal variability (Sperber and Annamalai 2008; Jourdain et al. 2013), the northwest–southeast-tilted rainband structure associated with low-frequency ISO is still missing in most of the models. And while many studies show that Atmospheric General Circulation Models (AGCMs) are capable of simulating realistic ISO variability (Waliser et al. 2003; Rajendran et al. 2008), there is a growing school of thought that air-sea coupling is necessary to reproduce more realistic ISOs over the Indian domain (Pegion and Kirtman 2008; Wang et al. 2009b; Sharmila et al. 2013; Misra et al. 2018). For example, Misra et al. (2018), using a high-resolution regional coupled ocean-atmosphere model with the lateral boundaries forced by global reanalysis datasets, showed a remarkable signature of low-frequency ISV patterns over India.

Despite the fact that onset/demise and ISOs are a vital part of the monsoon system, the linkage between the two phenomena have not been thoroughly studied, especially from a modeling perspective. Using a single, large-scale definition of an index of onset of the ISM using observed datasets, a few recent studies have been able to show the modulation of ISO on the onset (Wang et al. 2009a; Zhou and Murtugudde 2014). Wang et al. (2009a) defined an index

based on lower atmosphere zonal wind over the southeast Asia and they were able to show that northwestward propagation of convection from eastern equatorial Indian Ocean can influence the onset over Kerala. Using mean meridional temperature gradient to measure the land-ocean contrast as an index for the onset of the ISM, Zhou and Murtugudde (2014) found that northward propagating ISO plays a significant role in the occurrence of early onset of the ISM. However, they also found that a significant fraction of years have onset of the ISM without the modulation of ISO. In a recent observation-based study, Karmakar and Misra (2019) found that nearly 59% of local onset and 62% of local demise events occur during positive developing phases and positive decaying phases of two ISOs, respectively. Phase-locking between LF-ISO and HF-ISO is an important factor in determining the onset or demise events.

The purpose of this study is to bridge the gap between the knowledge concerning the two most prominent phenomena in the ISM, onset/demise and the ISOs, and to show how a regional coupled model is capturing the relationship between the two. The specific research questions are as follows:

- How are the onset and demise of the ISM associated with evolution of the ISO over the Indian region? Do particular phases of an ISO create a conducive environment for the onset or demise to occur? Here, instead of using a single index based on onset and demise, we define indices using a local grid point-based analysis in a data adaptive way. Additionally, the ISO structures are extracted from the data using a data-adaptive approach called Multichannel Singular Spectrum Analysis (MSSA).
- How are the space-time structures of the ISOs in the ISM in a regional coupled model simulated as compared to observation, especially in the 10–20-day mode, which has not been investigated properly in previous modeling studies? Additionally, we will investigate whether the model is reasonably simulating the seasonal cycle and onset and demise events of the ISM, for both AIR and at a local scale.
- How well does the model performs in capturing the relationship between the onset/demise of the ISM and both the ISO structures at a local scale?

Addressing these questions not only advances our understanding of the monsoon system, but also provides an essential diagnostic tool for anticipating the onset and demise of the ISM using the phase information of the ISOs. The performance of the model is also tested with a future aim of improving the predictability of onset/demise at a local scale using regional coupled models. The paper is organized as follows: Sect. 2 provides a brief description of the model, Sect. 3 introduces the dataset used in this study and describes how onset and demise of the ISM are calculated and ISOs are extracted from the rainfall data. Section 4 describes the results and Sect. 5 provides the conclusions and a short discussion on the results.

2 Model description and experimental design

The Regional Spectral Model (RSM; atmospheric component) coupled with Regional Ocean Modeling System (ROMS; oceanic component) is used in this study as the Regional Coupled Model(RCM) (Li and Misra 2014; Misra et al. 2017c, 2018). The RCM performs reasonably well in capturing the mean seasonal rainfall over the Indian region as well as the subseasonal variability (Misra et al. 2017c, 2018). The circulation patterns associated with the active-break cycle over India are well-simulated in the model. The RSM was first introduced in Juang and Kanamitsu (1994) and several modifications have been made to the model since then (Kanamitsu et al. 2010; Misra et al. 2018). It has 28 terrain-following sigma vertical coordinates. The ROMS has 30 vertical sigma levels on a horizontal staggered Arakawa C grid (Shchepetkin and McWilliams 2005). A summary of the physics used for the simulation is provided in Table 1. In this experiment, a 10 km grid resolution is used and the grids are identical for both the RSM and ROMS. This enables direct exchange of fluxes between atmospheric and oceanic components without the need for interpolation. The coupling between ROMS and RSM occurs in every three hours. Flux correction is not applied to the integration. The domain of integration is specified over the Indian region as shown in Misra et al. (2018) (roughly 4° N–37° N, 50° E–101° E; the simulations are performed over the entire region shown in Fig. 1c). Lateral boundary conditions for the RSM are

Table 1 Physics used in the RCM simulation

Physics	References
Atmospheric component (RSM)	
Deep convection	Moorthi and Suarez (1992)
Shallow convection	Tiedtke (1983)
Clouds	Zhao and Carr (1997)
Boundary layer	Hong and Pan (1996)
Land model	Ek et al. (2003)
Gravity wave drag	Alpert et al. (1988)
Longwave radiation	Chou et al. (1999)
Shortwave radiation	Chou and Suarez (1994)
Oceanic component (ROMS)	
Mixing scheme	Mellor and Yamada (1982); Umlauf and Burchard (2003)
Boundary layer formation	*K*-profile (Large et al. 1994)

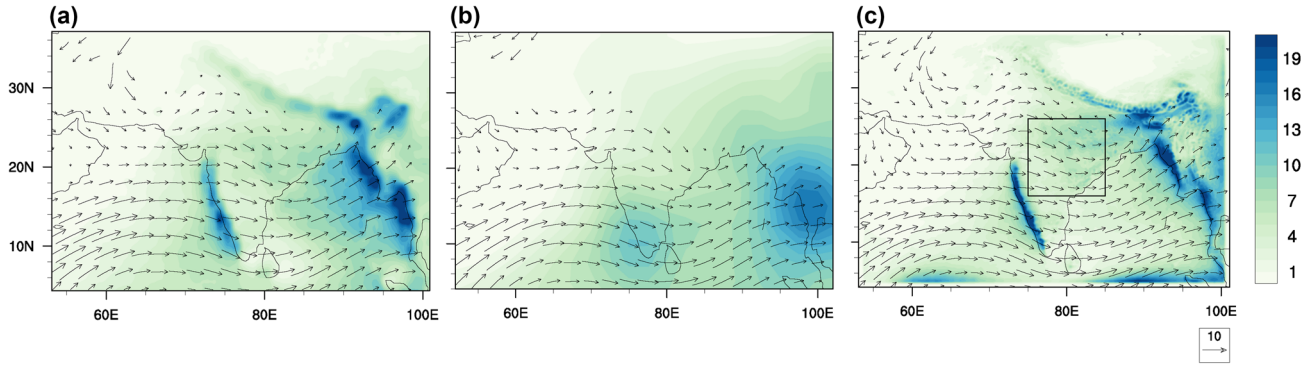

Fig. 1 **a** May–October seasonal mean rainfall from 1998 to 2014 obtained from TRMM 3B42 rainfall. Vectors represent mean 850-hPa winds for the same time period from ERA-Interim reanalysis. **b** Same as **a**, but from NCEP-DOE AMIP-II Reanalysis (R-2). **c** Same as **a**, but for 10 years of model simulation. The simulations are performed over the entire region shown in **c**. The smaller box shown in panel **c** marks the region based on which phase compositing is done in Fig. 2

prescribed by the National Centers for Environmental Prediction–Department of Energy global atmospheric reanalysis (Reanalysis-2) (Kanamitsu et al. 2002) every 6 h. The ROMS boundary forcings are from Simple Ocean Data Assimilation version 2.2.4 (SODA v2.2.4), global oceanic analysis (Carton and Giese 2008) prescribed at a monthly interval. The integration is carried out for a period of 10 years from January 1, 1986 through December 31, 1995.

3 Datasets and methodology

We use 0.25°× 0.25° gridded rainfall data from 1902–2005 obtained from India Meteorological Department (IMD) (Pai et al. 2014). Quality controlled data from 6955 rain gauge stations in India were used to construct this dataset, which has been used in many studies including Misra et al. (2017a). Grid points over the extreme northern portion of India are not considered in this analysis as rainfall over these regions may not be associated with monsoonal flow at times during the ISM, which can cause issues with diagnosis of local onset/demise of the ISM. We also use Tropical Rainfall Measuring Mission (TRMM) 3B42 (V7) daily rainfall data (0.25°× 0.25°) for 1998–2014 (Huffman et al. 2007). European Centre for Medium-Range Weather Forecasts (ECMWF) Re-Analysis (ERA)-Interim dataset (0.75°× 0.75°) (Dee et al. 2011) are also used for the same period (1998–2014). NCEP-Reanalysis 2 data provided by the NOAA/OAR/ESRL PSD, Boulder, Colorado, USA, from their Web site at https://www.esrl.noaa.gov/psd/.

The model output, which is at 10 km × 10 km resolution, is interpolated to the IMD grid for the subsequent analyses and only those points over which IMD data is provided are considered while grid points over the extreme northern region of the domain are removed. This is done to ensure a reasonable comparison between IMD observed rainfall and model output.

3.1 Defining the onset and demise dates

The onset of the ISM is defined as in Noska and Misra (2016) who stipulated daily cumulative anomaly of the AIR and ascribed the first day after the minimum in the daily cumulative anomaly as the onset of the ISM every year. The demise of the ISM is defined as the day after the maximum in the daily cumulative anomaly curve.

In this study, the local onset and demise dates are defined as described in Misra et al. (2017a), who first defined the climatological onset and demise over every grid point using the daily cumulative anomaly of the daily climatology, similar to how it is done for AIR. Next, using the daily cumulative anomaly of the daily climatological AIR, climatological onset/demise of AIR is also defined. Then the difference between climatological local and AIR onset/demise is calculated. Calculating this difference serves to average out the transients. Finally, local onset and demise of the ISM for every year is defined by finding the minimum and maximum values in the daily cumulative anomaly curve of the year in the immediate neighborhood of its climatological departure from AIR onset and demise, respectively. This approach to defining local onset and demise and anchoring it to AIR properties significantly reduces the possibility of detecting false onsets or demise possibly attributed to small-scale synoptic activities unconnected to the evolution of the ISM.

3.2 Extracting ISOs from rainfall data

A data-adaptive filtering technique called Multichannel Singular Spectral Analysis (MSSA) is used to extract ISO features from the rainfall data in observations and model (Plaut and Vautard 1994; Ghil et al. 2002). This

technique is used in various studies specifically to extract oscillatory signals from short and noisy time series. It is also used extensively in monsoon studies to understand the structure of intraseasonal variability in rainfall (Moron et al. 2012; Karmakar et al. 2017b; Karmakar and Krishnamurti 2018). The daily climatology at each grid point is removed from the data as a first step toward extracting ISOs. Since the observational data are 104 years long, the daily climatology is defined as the mean on each calendar day over the entire time period. On the other hand, model climatology is defined at each grid point using the first two harmonics (representing the annual and semiannual variations). This gives a smooth daily climatology based on only 10 years of data, which is removed from the daily data each year to obtain a daily anomaly. Next, a pre-filtering procedure is adopted with a five-day moving mean to remove very high-frequency fluctuations possibly attributed to synoptic activities. This data for each year is then fed into the MSSA algorithm to extract ISO modes.

Since the shape and bandwidth of the filters in MSSA are functions of the data rather than prescribed by the user, it provides a superior way to extract signal from noise and identify anharmonic oscillations in a nonlinear system. A lag-covariance matrix is constructed by augmenting lagged copies of the data. This matrix is then diagonalized to obtain space-time empirical orthogonal functions (ST-EOFs) and space-time principal components (ST-PCs). The eigenvalues provides an estimate of the power in these modes. If two consecutive eigenvalues are nearly equal and their associated ST-EOFs and ST-PCs are in phase quadrature, then these two eigenmodes represent an oscillation (Plaut and Vautard 1994). In this study, we use a lag window of 60 days while analyzing year-long data, which provides sufficient confidence to extract ISO modes in the data (Plaut and Vautard 1994). Additionally, a statistical test designed with 1000 red noise surrogates is used to eliminate the possibility of detecting random fluctuations as oscillations (Allen and Robertson 1996). Using the correct eigenmodes and associated ST-EOFs and ST-PCs, we can reconstruct the part of the time series that explains a periodicity in the preferred range: the reconstructed components (RCs). We define low-frequency ISO (LF-ISO) as the significant modes that have periodicity of 20–70 days. Similarly, high-frequency ISO (HF-ISO) is defined by the modes with periodicity ranging between 10 an d20 days. LF- and HF-ISO are defined using an approach similar to that used in Karmakar et al. (2017b) and Karmakar and Krishnamurti (2018). More details about the technique can be found in Ghil et al. (2002) and we refer to Karmakar et al. (2017b) for details about how the technique is used on Indian monsoon rainfall to extract ISO modes.

3.3 Defining the phases of an ISO mode

Based on the oscillatory behavior of the ISO modes (LF-ISO or HF-ISO), we can determine their phases using the following equation:

$$\gamma(t) = Arg(Y'(t) + iY(t)) \tag{1}$$

where, t denotes time calculated in days, $Y(t)$ is the n-day long LF-ISO or HF-ISO time series over a particular grid point, and ($'$) indicates the time-derivative calculated using central differences. $Y(t)$ and $Y'(t)$ are both normalized by their own standard deviations. $Arg(z)$ represents the principal value of the phase of a complex number $z = x + iy$. $\gamma(t)$ is calculated for each year individually. $\gamma(t)$ lies between $-\pi$ and π, and the phase plane can be divided into a number of equal intervals such that $-\pi + (m-1)\frac{\pi}{N} \leq \gamma(t) < -\pi + m\frac{\pi}{N}$, $m = 1, \ldots, N$, where N is the number of intervals ($N = 8$ is used here). Performing this analysis at each grid point allows us to reveal a more precise relationship between the ISO and the onset and demise of the ISM at local scales.

4 Results

4.1 Model performance in simulating monsoon

Figure 1a–c show the mean May–October rainfall and 850 hPa winds over the Indian region from observations (TRMM rainfall and ERA-Interim winds), NCEP- Reanalysis 2 (R-2) and model, respectively. Westerly low level winds are observed during the monsoon season with increased rainfall over the western Ghats, foothills of the Himalayas and Myanmar coast. Although low level winds in R-2 are in agreement with ERA-Interim, rainfall in R-2 is poorly represented over this region (see Figure S1 for bias). Only few parts over the southern India and Myanmar coast are observed to receive rainfall more than 10 mm/day. However, the model perform reasonably well in simulating the basic features of seasonal mean rainfall over this region. Rainfall over the western Ghats, foothills of the Himalayas and northern BoB experiences rainfall as in observation. Rainfall over central India is homogeneous and of similar magnitude as in observations (TRMM). Thus, compared to R-2, which is used as boundary forcings in the model simulations, the model performed far better in simulating the rainfall over the Indian region.

Intraseasonal features in the ISM rainfall is shown in Figs. 2 and 3 for both observations and the model. Based on the area averaged rainfall associated with LF-ISO or HF-ISO over central India, we calculate eight phases of ISO using the method described in Sect. 3 to show the

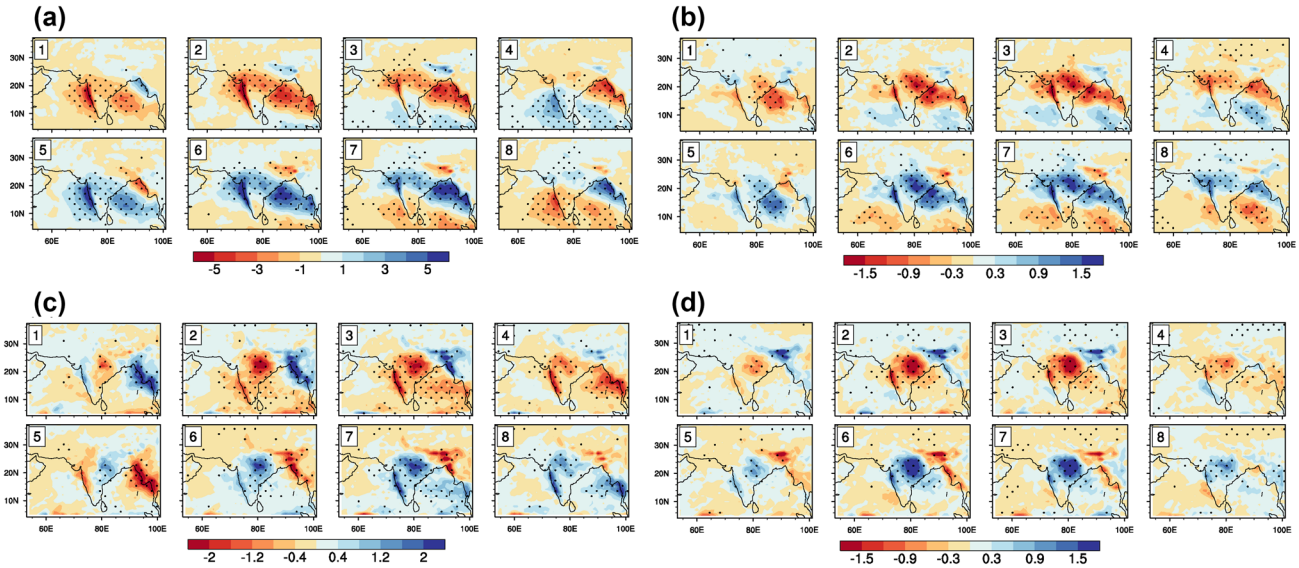

Fig. 2 **a** Phase composite diagrams of rainfall LF-ISO based on May–October, 1998–2014 TRMM 3B42 rainfall. **b** Same as **a**, but for HF-ISO. **c** Phase composite diagrams of rainfall LF-ISO based on May–October from 10 years of model simulated rainfall. **d** Same as **c**but for HF-ISO. Stippled areas indicate values are significantly different from 0 at 5% level using a randomization test. Phase numbers are noted in each of the panels. Phase composite for this diagram is done using an area averaged ISO over central India (16° N–26° N, 75° E–85° E; shown by the box in Fig. 1c) and divide the phase plane into eight intervals. However, all other analyses in this study are done by calculating the ISO phases at each grid point separately as discussed in Sect. 3

spatio-temporal evolution of ISO. Figure 2a shows the 104-year average of phase composite for LF-ISO obtained from observations. The eight phases are cyclic in order and are separated by an average of 4–5 days. In phase 1, a positive anomaly starts to develop over the southern Indian region, with most of central and peninsular India covered with a negative anomaly. In phase 2, the positive anomaly shifts slightly to the north and the negative anomaly gets established over central India. In the subsequent phases, the positive LF-ISO anomaly strengthens and moves northeastward and reaching central India and intensifying by phases 6 and 7. In phase 8, the positive LF-ISO band moves further northward and weakens over the foothills of the Himalayas. A northwest-southeast tilt in the convective band associated with LF-ISO is seen (phases 6 and 7). This canonical structure of LF-ISO has been documented in many previous studies (Krishnamurthy and Shukla 2007; Lee et al. 2013; Karmakar et al. 2017b).

The model captures this oscillatory behavior of the LF-ISO quiet well (Fig. 2c). The central Indian region shows strong positive anomalies in phases 6 and 7, which subsequently propagates northward and weakens over the foothills of the Himalayas. However, the northwest–southeast tilt in the convection is comparatively less prominent in the model than in the observations. Simulating this tilt in the rainband associated with LF-ISO is a difficult task, and many state-of-the-art models still fail to reproduce this band properly (Sabeerali et al. 2013). Figure 2c shows that RCM is capable of capturing the magnitude of the LF-ISO anomalies over the Indian region.

Figure 2b, d show the spatio-temporal evolution of HF-ISO in phase composites for the observations and model, respectively. The dominant structure associated with HF-ISO is linked with a northwestward propagation of convection from the east coast of India to the northwestern region (Rajasthan) (Karmakar et al. 2017b). The eight phases shown in Fig. 2b are nearly 2–3 days apart from each other. Both the model and observations show a development of a positive anomaly over the eastern coast in phases 4 and 5. This anomaly gradually propagates northwestward while intensifying in phases 6 and 7. In phases 8 through 2 (the eight phases are cyclic in order), this moves further westward and dissipates over the northwestern India. The model performs reasonably well in capturing the northwestward propagation of convection associated with HF-ISO in terms of magnitude and spatial scale (Fig. 2b).

Propagation characteristics of rainfall in both observation and model can be better understood using phase-latitude diagrams shown in Fig. 3. Figure 3a, b show northward and westward propagation of rainfall anomalies over India associated with LF-ISO and HF-ISO, respectively. Northward propagation of LF-ISO along the BoB longitudes from the equatorial Indian Ocean in phase 2 to the foothills of the Himalayas in phase 8 can be seen. Westward propagation of rainfall anomalies in HF-ISO timescale along the central Indian latitudes from nearly 100° E to 70° E is also observed

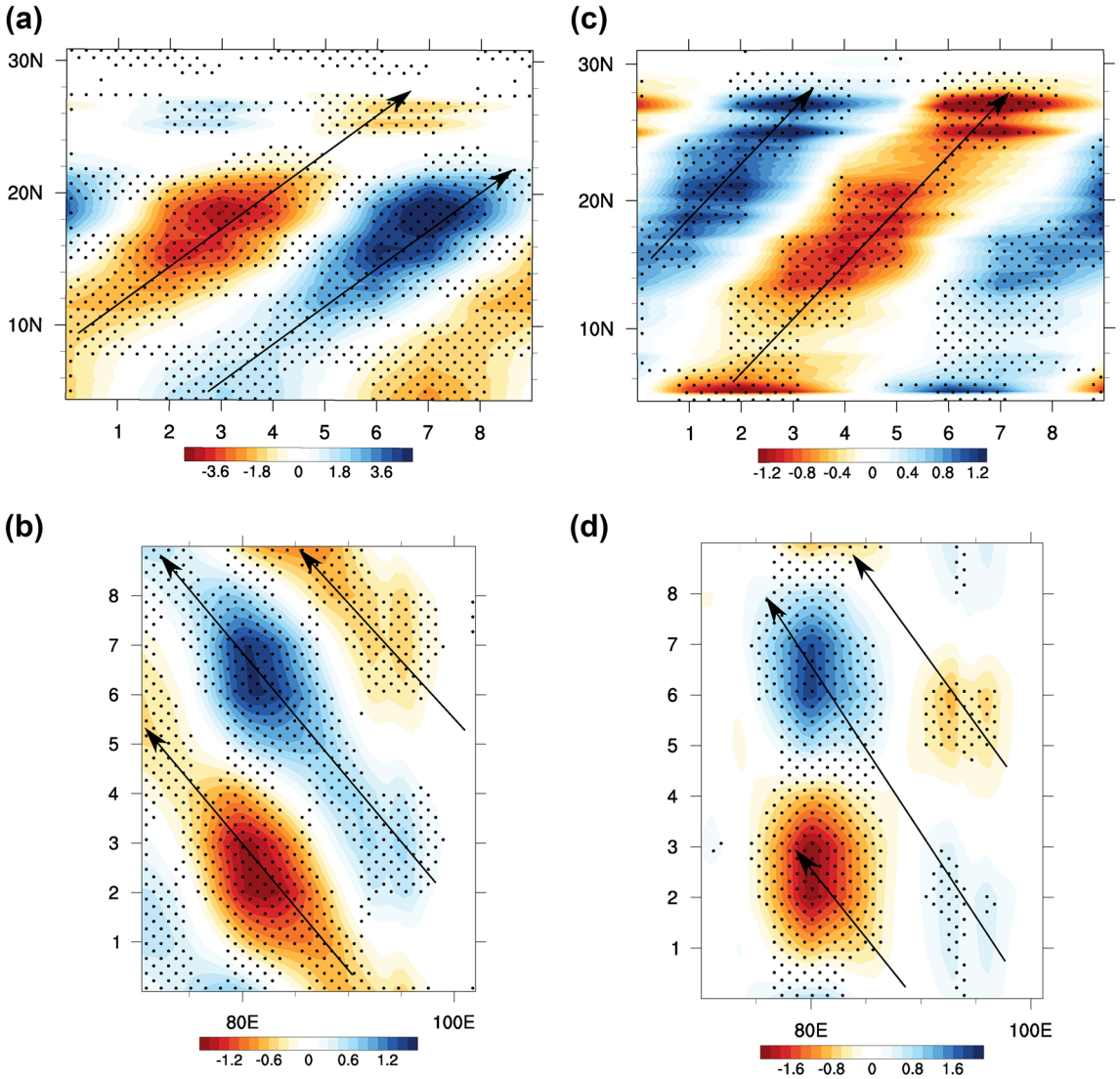

Fig. 3 **a** Northward propagation (marked by arrows) of May–October LF-ISO rainfall anomalies from TRMM 3B42 rainfall represented in phase-latitude composite diagram. Longitudinal averaging is done across 85°–95° E. **b** Westward propagation of May–October HF-ISO filtered v-wind anomalies at 850 hPa level ERA-Interim reanalysis represented in longitude-phase composite diagram. Latitudinal averaging is done across 15° N–20° N. **c, d** Same as **a** and **b**, respectively, but for 10 years of model data. Units of rainfall and winds are *mm/day* and *m/s*, respectively. Stippled areas indicate values are significantly different from 0 at 5% level using a randomization test

between phases 2 and 8. The model shows both northward propagation and westward propagation remarkably well (Fig. 3c). However, there is a difference in phase of rainfall associated with LF-ISO between the model and observations over the BoB longitudes. Rainfall over the northern BoB (20° N) shows maximum value at phase 2 in the model compared to phase 7 in observation. This could possibly be related to the difference in phase relation between rainfall over central India and BoB in model and observation. Westward propagation associated with HF-ISO are often initiated form the west Pacific and shows a double cell structure at the lower atmosphere (Chen and Chen 1993; Karmakar and Misra 2019). Although the model domain is restricted to roughly 101° E in the west, the model also captures westward propagation associated with HF-ISO reasonably well (Fig. 3d).

4.2 Local onset/demise and ISO phases

Figure 4a, b show the climatological local onset and demise dates from observation based on 104 year-long IMD rainfall data. The progression and retreat of the typical monsoon isochrone between the southern part and the northwest of India is observed in the two figures. Parts of Kerala experiences onset as early as in the third and fourth week of May. Onset is observed during middle of June over the

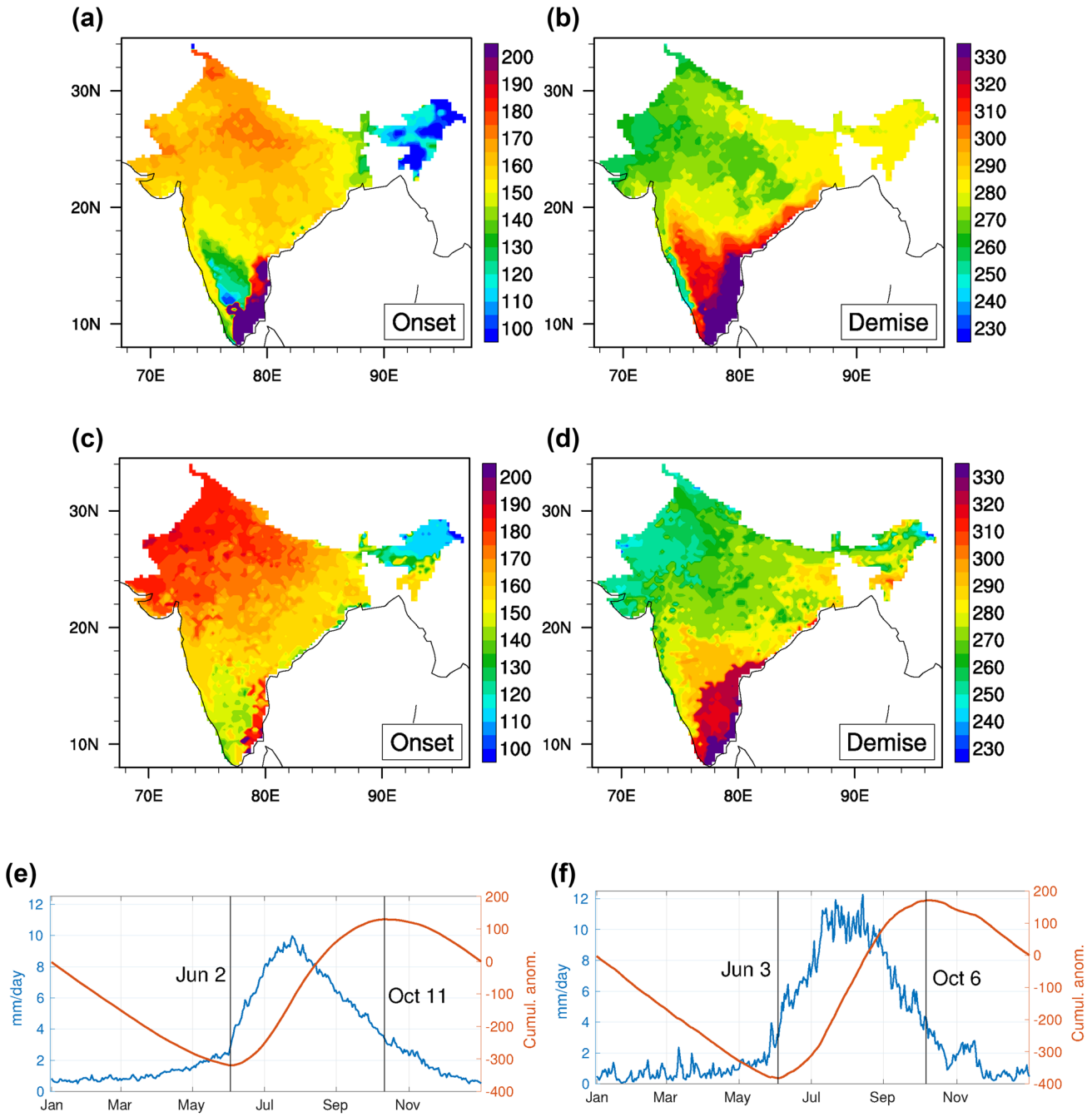

Fig. 4 The climatological **a** onset and **b** demise of the Indian summer monsoon (ISM) defined at every grid point of the IMD gridded rainfall data from 1902 to 2005. **c**, **d** Same and **a**, **b**, but for 10 years of model simulation. The dates are shown in Julian days. **e** Daily climatology of the All-India rainfall (AIR; left *y*-axis in blue) from the observed rainfall data from Indian Meteorological Department (IMD) and the corresponding cumulative daily anomaly (right *y*-axis in red) with the onset and demise dates marked in calendar days. **f** Same as **e**, but for model

central Indian region. Regions over south-western peninsular India (Tamilnadu) experience a very delayed onset, as the majority of rainfall over this region is associated with the northeast monsoon (Rajeevan et al. 2012). However, onset occurs very early (as early as mid-April) over few a regions including central peninsular India (Karnataka) and northeast of India. Onset over the northeastern states also occures much earlier before the onset of the ISM (Wang and LinHo 2002). The onset over these regions is often related to pre-monsoon showers and the transition from pre-monsoon showers to summer monsoon rains occurs rather smoothly (Krishnamurti and Ramanathan 1982; Misra et al. 2017a).

This smoothness leads the algorithm to detect the onset over these regions very early. It is also argued that the pre-monsoon showers could be a necessary precursor to the summer rains over these regions (Misra et al. 2017a). Thus, they are important in understanding the evolution of the ISM. Since onset is determined based on identifying a smooth monotonous increase in rainfall amount over a location, this leads the algorithm detect the onset over these regions very early. Defining onset and demise of the ISM on a local scale in this manner has particular importance to anticipate the evolution of the ISM from early onset over parts of peninsular and northeast India.

The climatological local demise over central India is observed during late September, with the northeastern and peninsular Indian regions experiencing the demise mostly by early and late October, respectively. This delayed demise makes the length of the monsoon period over these regions longer than it is over central India. The delayed demise over peninsular India is associated with the rainfall during the north–east monsoon. The climatological local onset and demise of the ISM in the model simulation is shown in Fig. 4c, d, respectively. The comparison of the progression of the isochrones in the observations (Fig. 4a, b) and model simulation (Fig. 4c, d) show significant similarity. For example, the model simulation shows onset over central India (Fig. 4c) nearly the same time as observations (Fig. 4a). Similarly, the early onset over the northeast and peninsular India and late onset over the southwestern peninsula are also seen in the model. But the onset of the ISM over northwest India is slightly late in the model. Additionally, the climatological local demise dates in the model simulation (Fig. 4d) show resemblance with the corresponding dates from the observations.

Figure 4e, f show the daily climatology of AIR from observations and model, respectively, along with the daily cumulative anomalies. The model performs reasonably well in capturing the annual cycle of rainfall over India, showing rainfall picking up during early June, maxima in the late July to early August period, and then a gradual weakening. Based on the cumulative anomalies, the climatological AIR onset date is June 2 in the observations and June 3 in the model. Climatologically, AIR onset occurs later than onset over Kerala as AIR onset is calculated while combining all the data points over Indian land in the analysis. Most of central and western India experiences onset during and after the first week of June. The demise date is estimated as October 11 in the IMD rainfall data, while the model shows the demise date five days earlier. Considering the fact that the model analysis is done only for 10 years, in contrast to 104-year long observations, this is a reasonably good performance by the model in producing the climatological AIR onset and demise.

How do LF-ISO and HF-ISO propagation modulate the local onset/demise events over India? To answer this question, we looked into the local onset and demise events every year at each grid point and identify the LF-ISO and HF-ISO phases as shown in Fig. 2a, b, respectively, during onset/demise events. In Fig. 5a, we show the percentage of the total local onset events at each grid point during 104 years that occurred during each of the phases, where the phases of LF-ISO are calculated using rainfall averaged over central India as described in Fig. 2a. Clearly, during phases 5 and 6 of LF-ISO as in Fig. 2a, when wet phase LF-ISO is approaching central India, percentage of occurrence of local onset over most of central and northern India is very high. Nearly 40–50% of total onset events over central India occur during phases 5–6. Moreover, as LF-ISO propagates northward as in Fig. 2a, progression of the onset isochrone can be seen from phases 1 to 8 in Fig. 5a. This suggests that the LF-ISO propagation may have a strong role in determining the local onset over India. Phase 2 in Fig. 5a shows high percentage values over central-eastern and peninsular India, which could be linked to a simultaneous arrival of HF-ISO wet phase (Karmakar et al. 2017b). This could also be related to the fact that the ISO phases are defined based on central India in this context. Which means that phases 5–6 over central India could be associated with wet phase over peninsular India and northeast India. The model also captures the behavior reasonably well (Fig. 5b). Central India exhibits significantly large percentage values of local onset during phases 5 and 6. Onset over the western parts of India occurs in phases 7–8. HF-ISO phases as calculated in Fig. 2 shows comparatively weaker association with the local onset/demise events (Figure S2). However, local demise events over most of central and eastern India largely occur during phases 7–8 of LF-ISO and HF-ISO (Figures S3, S4).

However, calculating the ISO phases using a domain average rainfall can have some biases and may not exhibit the correct relationship between the onset/demise events and ISO phases. In order to find a relationship between the local onset and demise each year and ISO phases, we divide the LF-ISO and HF-ISO at each grid point into 8 phases using the methodology described in Sect. 3. In Fig. 6, we show how this is done using an example over a location in central India (21° N, 79° E). Figure 6a, b show LF-ISO and HF-ISO, respectively, along with their phase angles over this grid point for 1986, respectively. Figure 6c shows the actual rainfall during the same time period, which reveals that the peaks in actual rainfall are marked by simultaneous occurrences of strong positive values of LF- and HF-ISO. Their phase-locking results in a strengthened active rainfall spell over the location (Karmakar et al. 2017b). Similar characteristics are seen in the model data over the same location as well in Fig. 6d–f.

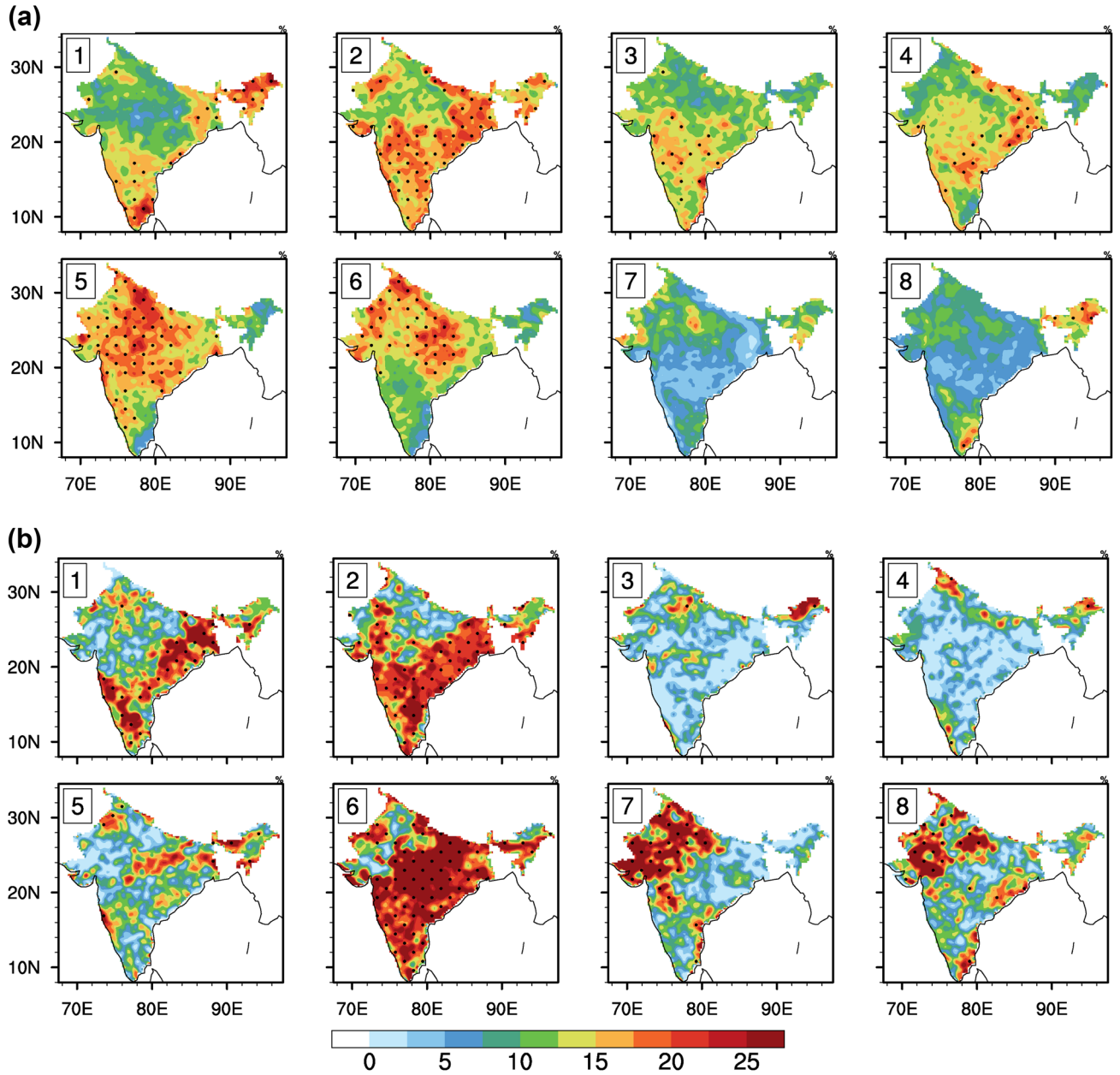

Fig. 5 **a** Percentage of local onset from observation (IMD) occurring in each of the phases of LF-ISO as calculated using the area-averaged rainfall over central India using IMD rainfall data. Spatial maps of the phases of LF-ISO using this technique is similar over Indian land as described in Fig. 2a in the main document. **b** Percentage of local onset from model simulations occurring in each of the phases of LF-ISO as calculated using the area-averaged rainfall over central India using IMD rainfall data. Spatial maps of the phases of LF-ISO using this technique is similar over Indian land as described in Fig. 2a in the main document. Stippling indicates values which are significant at 5% level using a one-sided bootstrapping test

The local onset and demise dates over the same grid point are also marked in each panel. The dotted lines in the panels (a)–(d) show the phase associated with the respective ISOs. The phase lies between $-\pi$ to π, which is divided into 8 equal intervals. This is done for all of the grid points and all years used in the analysis. Phases 1 through 4 show the negative values of the ISO while phases 5–8 show positive values. On the other hand, phases 3–6 exhibit a developing phase of ISO, whereas phases 7–2 show a decaying phase.

The next goal is to identify the local onset and demise dates every year at each location, and then find the phases of LFISO and HF-ISO in which these dates are falling. If the local onset or demise dates show preferred phases of ISO, that would imply the onset or demise of the ISM is synchronized with large-scale oscillatory spatio-temporal patterns

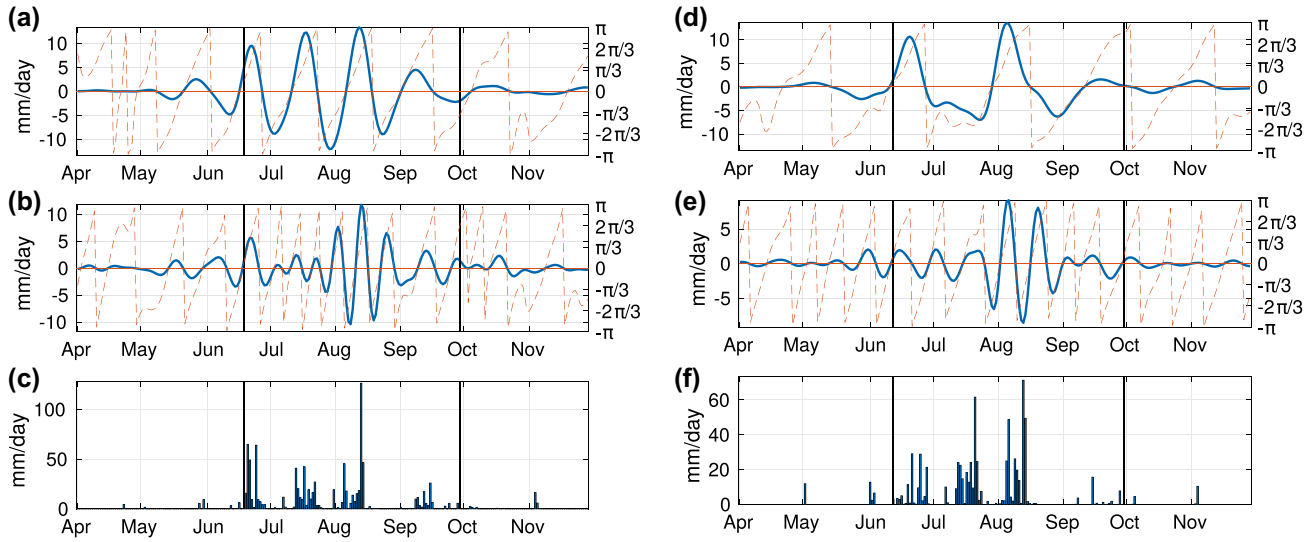

Fig. 6 **a** LF-ISO (left *y*-axis; solid line) over a grid point over central India (21° N, 79° E) during April–November, 1986 (from IMD gridded rainfall observation). Right *y*-axis shows the phase angle (dashed red line) for the same time period calculated as described in the text. **b** Same as **a**, but for HF-ISO. **c** Actual observed rainfall for the same time period over the same location. Local onset and demise dates in 1986 over the same location are shown as vertical lines in all the panels. **d–f** Same as **a–c**, but for model

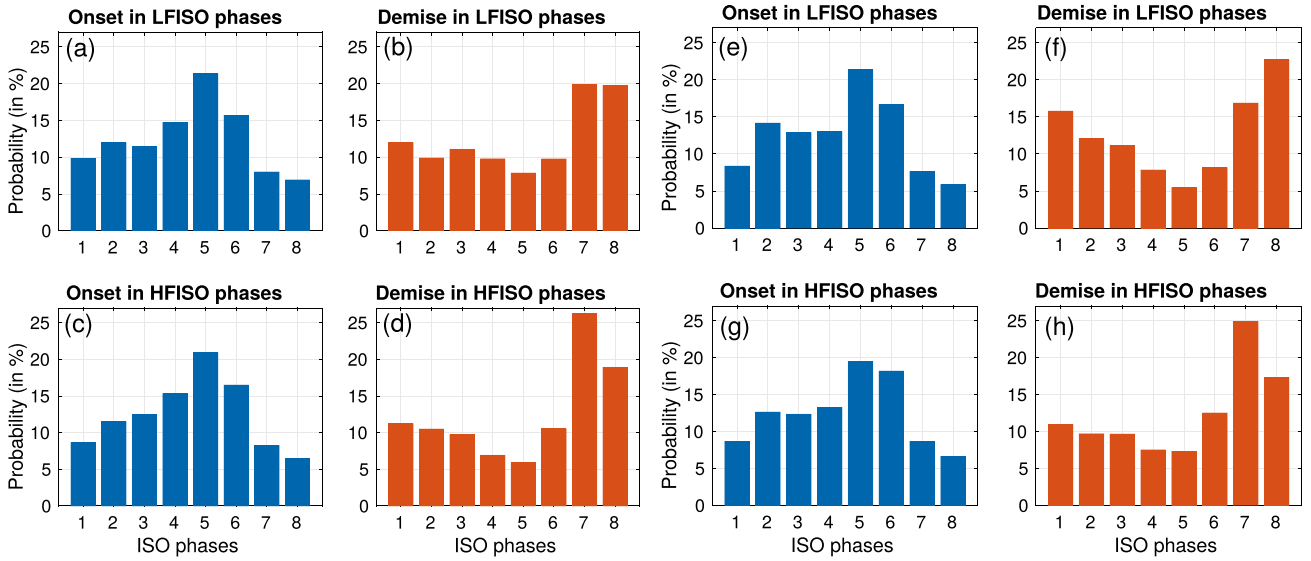

Fig. 7 **a** Histogram of local onset dates of the ISM (presented as a percentage of the total) in different LF-ISO phases as calculated using the IMD rainfall data. All the grid points taken in the analysis over the Indian domain and all the years of data (1902–2005) are considered to create the histogram. *x*-axis represents different LF-ISO phases. **b** Same as **a**, but for local demise dates of the ISM. **c** Same as **a**, but for local onset dates of the ISM in HF-ISO phases. **d** Same as **c**, but for local demise dates of the ISM. **e–h** Same as **a–d**, but for 10 years of model simulation

of convection and thus can be estimated apriori if proper information about the ISO phases are provided.

Figure 7 shows the distribution of the occurrences of local onset and demise dates in different LF-ISO and HF-ISO phases for the IMD rainfall data using 104 years. Figure 7a show that local onset is highly probable when the LF-ISO is in phases 5–6 (positive developing stage). Nearly 37% of all the local onset occurrences across India are confined to these phases, suggesting onset over a location is highly preferable when LF-ISO exhibits positive or slightly negative rainfall anomaly values with an increasing tendency. Similarly, local demise dates are concentrated in LF-ISO phases 7–8 (positive decaying phase), with almost 40% of the total local demise dates falling within these four phases

(Fig. 7b). Nearly 37% of the total cases of local onset and 45% of the total cases of local demise occur when the HF-ISO exhibits a developing phase (phases 5–6) and positive decaying phase (phases 7–8) (Fig. 7c, d). A stronger relationship between the local demise with HF-ISO phases as compared to LF-ISO phases is seen. Importantly, the preferred phase for demise is not the negative phase of ISO, but rather, demise occurs primarily during the positive phase with decaying characteristics.

A similar diagram of the distribution of the occurrences of the local onset and demise dates in different ISO phases for the 10 years of model output is shown in Fig. 7e–h. Interestingly, the model captures the features of preferred ISO phases for onset/demise quite well. In fact, the histograms look nearly identical with almost 39% of the total local onset cases and 40% of the total demise dates falling within preferred LF-ISO phases (developing phases 5–6 for onset and positive decaying phases 7–8 for demise) (Figs. 7e, 8g). Nearly 38% and 42% of the local onset and demise dates fall in the preferred HF-ISO phases, respectively (Figs. 7f, 8h). This is remarkable as the model not only captures the climatological progression of local onset and demise dates (in Fig. 2) and ISO characteristics in both high- and low-frequency ranges but also the synchronization between the two phenomena of onset/demise of the ISM and ISO modes.

The above discussion shows how LF-ISO and HF-ISO modulate the local onset and demise individually. The simultaneous modulation of these two ISO modes is more revealing when we observe the joint probability distribution of the local onset and demise dates in different LF- and HF-ISO modes as shown in Fig. 8. Figure 8a, b show the joint probability distributions for local onset and demise in 8 different

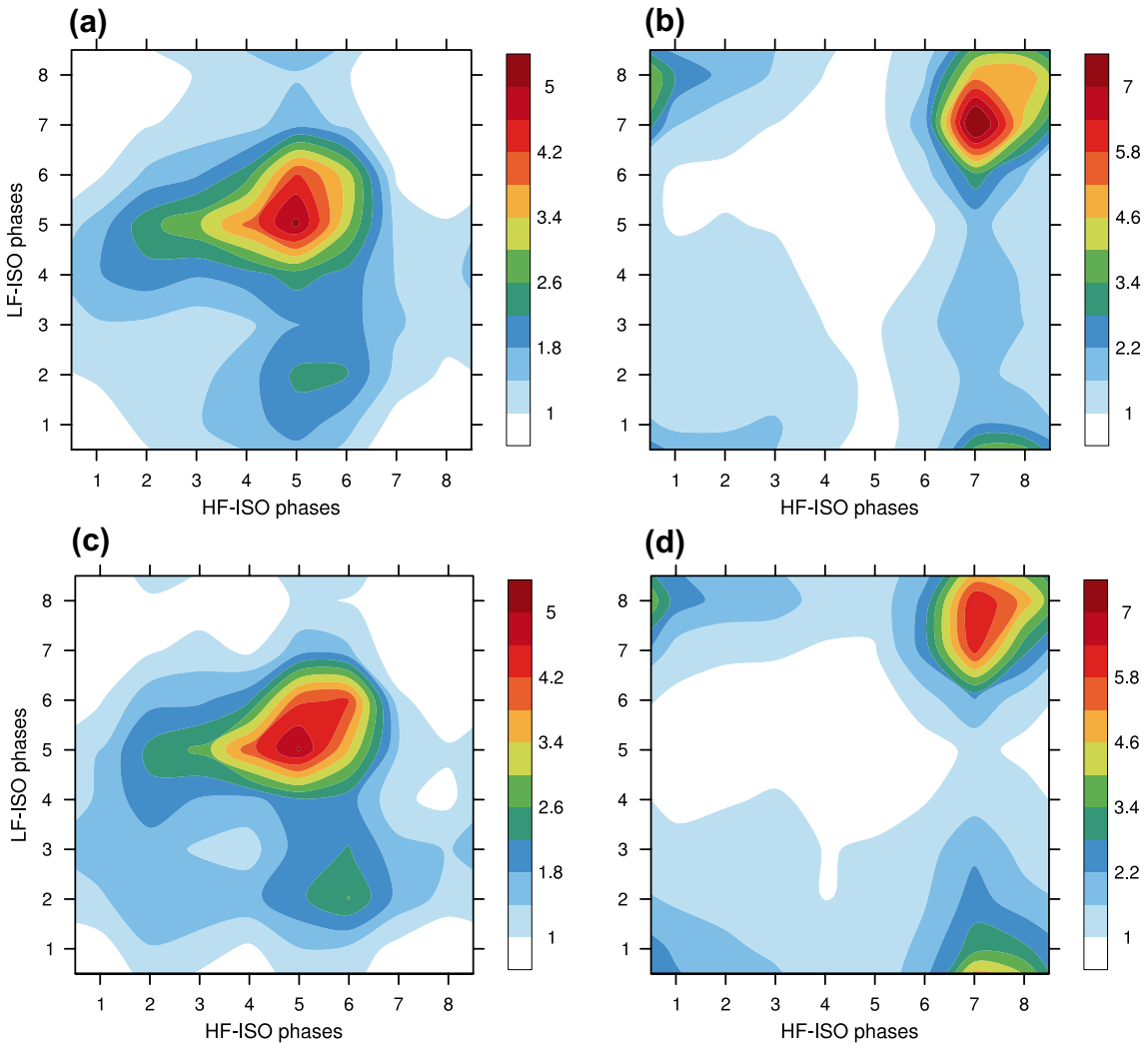

Fig. 8 Joint probability distribution (represented as percentage of total occurrences) of the local **a** onset and **b** demise dates of the ISM over the entire domain during 1902–2005 using IMD rainfall data in different LF-ISO and HF-ISO phases. **c**, **d** Same as **a**, **b**, but for model simulation (1986–1995)

phases of LF-ISO and HF-ISO using IMD rainfall data, respectively. The local onset is most probable when both the ISO modes are in phases 5–6, during the positive developing phase, having stronger alignment with the developing phases of LF-ISO. The contour plot indicates that the onset of the ISM over a location is most probable when both the ISO modes show developing stages of their evolution. This suggests that the onset of the ISM over a location highly depends upon the simultaneous occurrences of wet rainfall anomalies associated with the two ISO modes. Both of the ISO modes contribute almost equally for the occurrence of local onset; however, local demise events are more aligned to the HF-ISO phases 7–8. This suggests that the local demise is more concentrated within the positive decaying phases of HF-ISO as compared to LF-ISO. The model shows similar characteristics of the joint probability distribution to those in the IMD rainfall data (Fig. 8c, d). The developing phases of HF-ISO that coincide with LF-ISO phases 5–6 represent the most probable stage for the onset to occur at any location in the model. The demise dates are also concentrated within the positive decaying phases of both the ISO modes.

The joint probability plots presented in Fig. 8 suggests that phase-locking could be an important factor in triggering onset/demise over a location. In fact, nearly 15.7% of the observed local onset events are associated with the simultaneous occurrence of phases 5–6 for both LF-ISO and HF-ISO (Fig. 9a). Whereas, almost 22.7% of the observed local demise events are linked with the time when both LF-ISO and HF-ISO simultaneously are in phases 7 and 8 (Fig. 9b). Although the percentage values appears to be small, they represent the fact that out of 64 (8 LF-ISO phases × 8 HF-ISO phases) combination, only 4 can explain 15.7% of the local onset and 22.7% of the local demise. The model captures these features reasonably well. 16.8% of the total local onset events in the 10 years of model simulation over India occurred when both ISOs are in phases 5 or 6. Also, 20.5% local demise events occurred during simultaneous occurrence of phases 7 or 8 of LF-ISO and HF-ISO. Set-theoretic calculations lead to the fact that 58.8% observed local onset events are associated with either of the ISOs in phases 5 or 6. Similarly, 62.1% local demise events occur within phases 7 or 8 of either LF-ISO or HF-ISO. These numbers are quite accurately captured by the model with nearly 58.9% of total local onset occurred in when either LF-ISO or HF-ISO is in phases 5 or 6 and almost 61.4% local demise over India are occurred within phases 7 or 8 of either LF-ISO or HF-ISO.

The spatial pattern of this apparent synchronization of onset or demise events with the LF-ISO mode in the IMD and model rainfall data is shown in Fig. 10. Figure 10a shows the the peaks (maximum values) of the distribution of LF-ISO phases at which onset of the ISM occurred at each location over India in 104 years of observed rainfall data. As expected, most of the Indian region shows local onset of the ISM at phases 5–6 of LF-ISO, suggesting that the onset over almost all of India occurs during positive developing stage of LF-ISO over that location. A few regions, such as over eastern India, show peaks in the onset date distribution during LF-ISO phases 2–3. Although the model is restricted

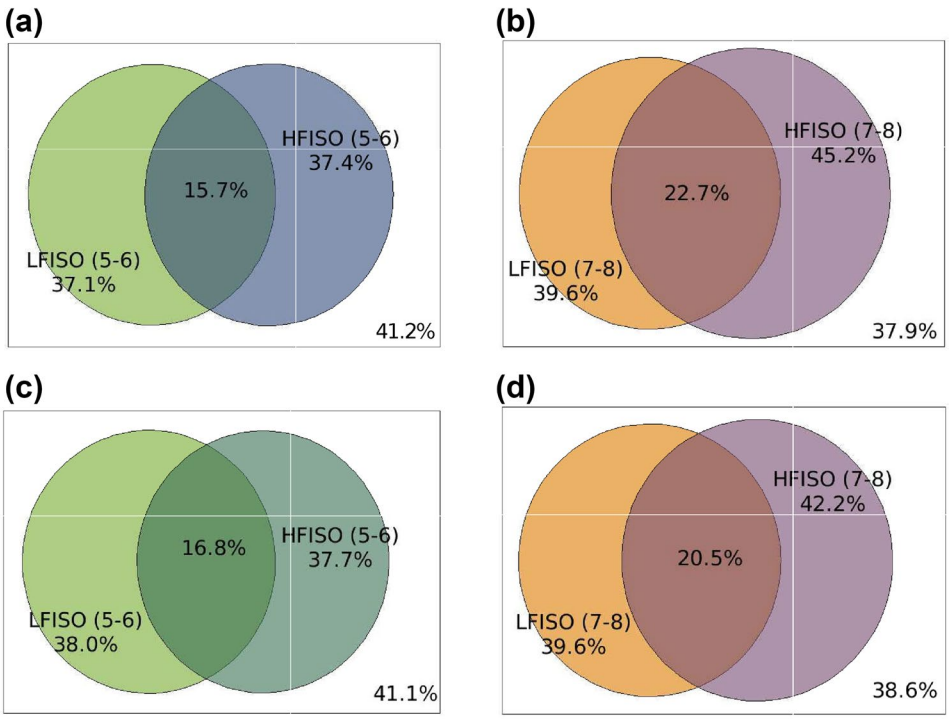

Fig. 9 Venn diagrams representing the percentage of occurrence of **a** local onset and **b** local demise over the entire domain in favorable LF-ISO and HF-ISO phases (phases 5 and 6 for local onset and phases 7 and 8 for local demise of the Indian summer monsoon) using IMD rainfall data from 1902 to 2005. **c**, **d** Same as **a**, **b**, respectively, but for 10 years model simulation. Values in the lower-right corner in each panel represent the percentages of local onset/demise which have not occurred during favorable ISO phases

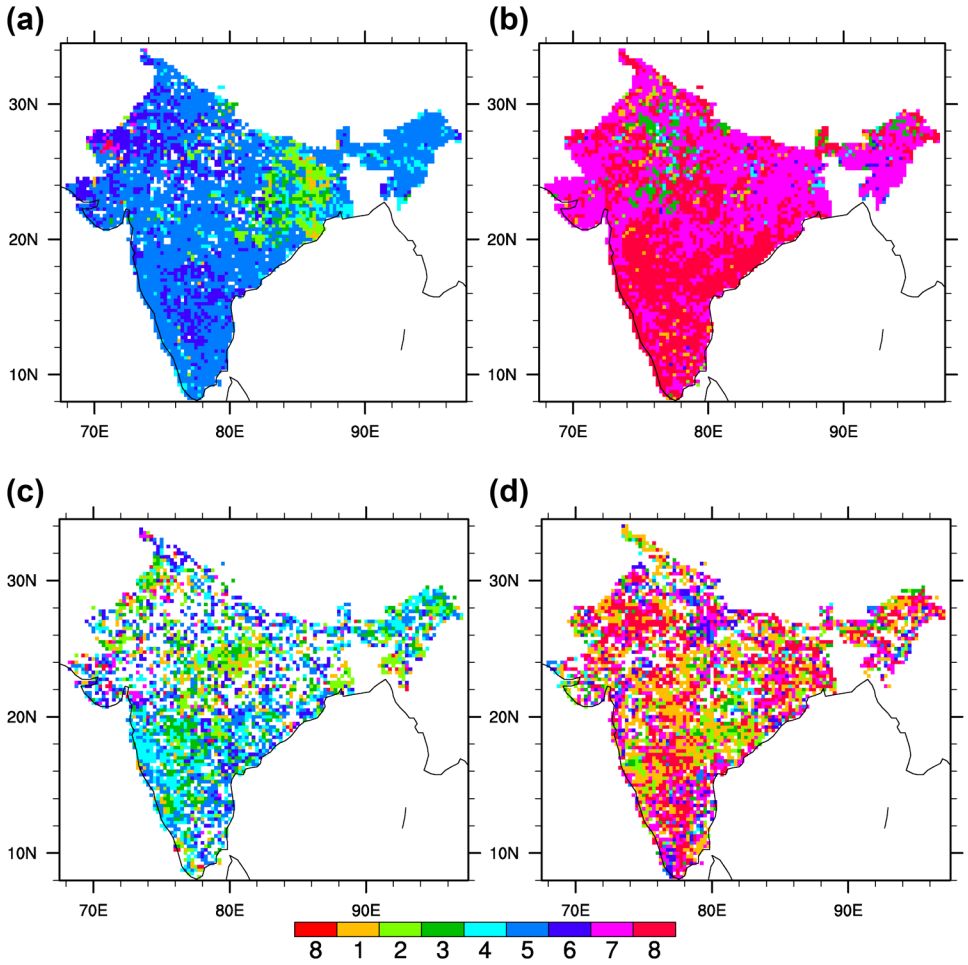

Fig. 10 **a** The spatial distribution of the LF-ISO phase numbers at which the distribution of local onset dates in different LF-ISO phases during 1902–2005 in IMD rainfall data attains maxima. **b** Same as **a**, but for the local demise dates. **c**, **d** Same as **a**, **b**, but for 10 years of model data. Only those grid points are shown in where the distribution of phases reject the null hypothesis of a uniform distribution at 5% significance level using Kolmogorov–Smirnov Goodness-of-Fit test

with only 10 years data, it captures the spatial distribution reasonably well and shows peaks in the distribution almost everywhere in India during developing phases of LF-ISO (Fig. 10c). Pattern correlation between maps in Fig. 10a, c is 0.90. There are few locations, particularly over central India, where local onset occurrences of the ISM are distributed among LF-ISO phases 2–3. The demise dates also show a coherent spatial pattern in the IMD rainfall with nearly the entire India exhibiting most preferred LF-ISO phases 7–8 (decaying stage), the exceptions being a few regions over the northwestern India (Fig. 10b). Although the model captures the spatial pattern reasonably well (Fig. 10d; pattern correlation between Fig. 10b and d is 0.83), there are few regions over central India that show the most preferred LF-ISO phase during demise of the ISM as negative developing phases (phases 1–2).

Figure 11 shows the spatial patterns of the preferred HF-ISO phases during the onset and demise of the ISM for both observed and model rainfall data. With the exception of a few regions over central India and the western Ghats, onset in the observation over India occurs mostly during positive developing phase of HF-ISO (Fig. 11a). The demise of the ISM over most of India, apart from a few regions (e.g., northeast India), occurs when HF-ISO shows a positive decaying phase (phases 7–8). The model captures these features reasonably well except for some regions over central, peninsular, and northwest India, which exhibit a most preferred phase during onset as phases 4–6 (Fig. 11c; pattern correlation between the maps in Fig. 11a and c is 0.90). Demise dates are mostly embedded within the HF-ISO phases 7–8 across entire India (Fig. 11d; pattern correlation between the maps in Fig. 11b and d is 0.91). We note that, despite the fact that the model data is limited to only 10 years, the probability distribution of the local onset and demise dates in different phases of ISO modes closely follows the observation and captures the spatial patterns reasonably well.

5 Conclusions and discussions

In this study we examine the relationship between the local onset and demise of the ISM and the intraseasonal features observed in the ISM using observed rain gauge analysis over

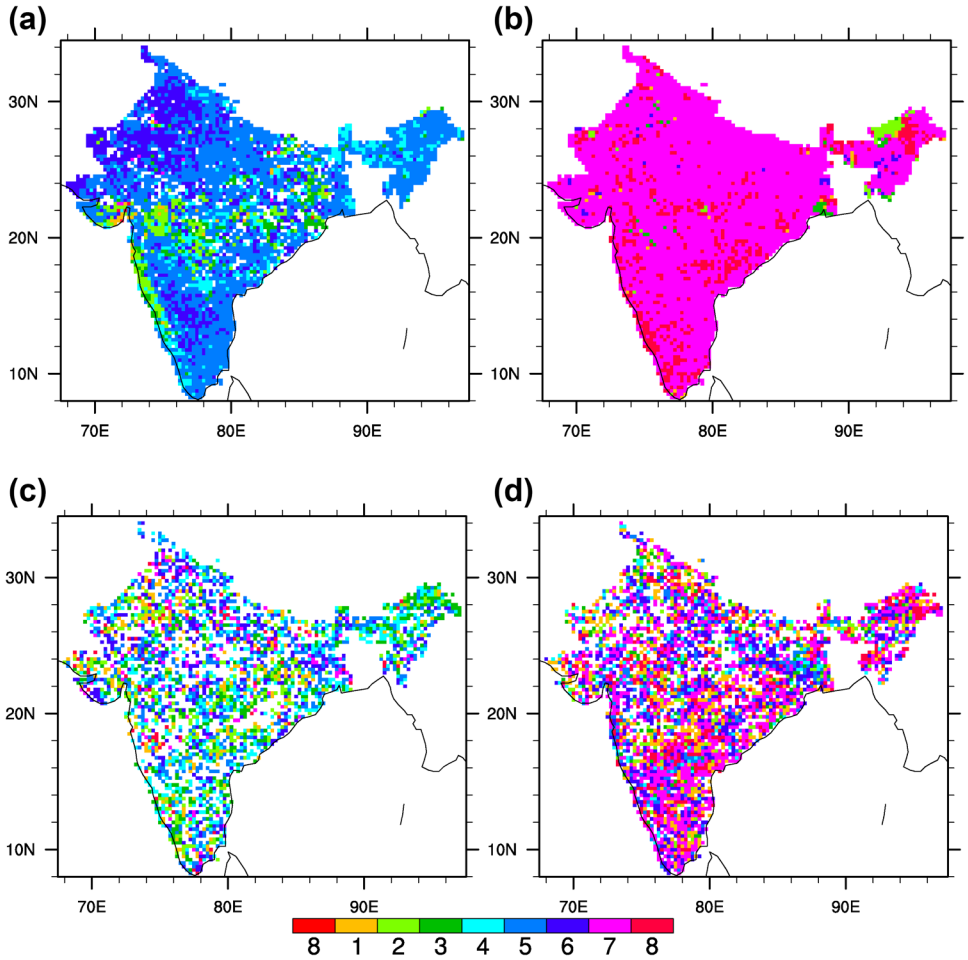

Fig. 11 **a** The spatial distribution of the HF-ISO phase numbers at which the distribution of local onset dates in different HF-ISO phases during 1902–2005 in IMD rainfall data attains maxima. **b** Same as **a**, but for the local demise dates. **c**, **d** Same as **a**, **b**, but for 10 years of model data (1986–1995). Only those grid points are shown in where the distribution of phases reject the null hypothesis of a uniform distribution at 5% significance level using Kolmogorov–Smirnov Goodness-of-Fit test

the Indian subcontinent for 104 years and a regional coupled model simulation of 10 years. In other words, we investigate whether onset and demise of the ISM are linked with the large-scale convective features in the monsoon and whether these characteristics can be captured by a regional model simulation. The local onset and demise dates of the ISM are defined based on calculating the inflexion points in the cumulative rainfall anomaly at each grid point and anchoring it to the AIR anomaly. The ISO structures are extracted using MSSA, a data-adaptive non-parametric method. The salient feature found in this study is the physical relationship found between the onset and demise of the ISM and ISO modes. We find that the local onset and demise of the ISM over a large fraction of the area over India is modulated by the ISO modes. This influence of the ISO is manifested by local onset occurring (58.8%) in positive and developing phases of both HF- and LF-ISO, which represent phases of the ISO when the positive rainfall anomalies are growing to their peak value. Similarly, the role of ISO evolution on the local demise of the ISM is diagnosed when 62.1% of the demise dates fall within ISO phases 7–8, phases of the ISO when the rainfall anomalies are diminishing from its peak positive values. However, there are significant areas within the core of the monsoon zone (central India) where both the local onset and demise of the ISM occur in other relatively unfavorable phases of the ISO, which may have potential implications on predictability and prediction strategies for local onset and demise of the ISM. In distinguishing the roles of HF-ISO and LF-ISO, we indicate that the former has a slightly more dominant influence than the latter on the local onset (especially over eastern and central India) and demise (over the northwestern regions) of the ISM. However, we do not find any correlation beteen the number of onset/demise evets occurring in favorable ISO phases and the intensity of ISO within a season (see supplementary Figures S5 and S6). Perhaps nature of ISO during the beginning and the end of the season could be different from the rest of the season. This warrants further investigation on how ISO intensity changes within a season and how it affects the onset/demise in a local scale.

The model performs well in capturing the basic nature of onset and demise at a local scale and how they link with the ISO phases. The model not only captures the seasonal cycle and ISO structures reasonably well, but it also shows

the correct phase relationships between onset/demise of the ISM with the ISO modes. These results imply the potential for predictability of the local onset and demise of the ISM. The study demonstrates the possibility of predicting the local onset and demise of the ISM when the phase information of the ISO modes are simulated reasonably well in the model. This leads us to suggest that the linkage between the onset and demise with the slowly varying intraseasonal modes in the monsoon could be exploited to develop targeted predictions of the onset and demise of the ISM. Such an advance in our understanding of the ISM would have practical applications and significant implications for the agro-economic society of India. The model, with its high-resolution simulation of the ISM, has already been proven to produce improved spatiotemporal structures of the LF-ISO mode associated with active-break spells (Misra et al. 2018). The findings in this study increase our confidence in this model to examine the vagaries of the ISM and indicate that if we can improve the basic structures of the ISO modes, prediction of the seasonal phenomena (such as onset and demise) can be further refined. In this regard, the model we use in this study simulates the ISO structures very well, especially the northward moving patterns in LF-ISO and northwestward propagating patterns in HF-ISO. Even the state-of-the-art global models remain limited in their ability to simulate the basic structures of LF-ISO modes (Sabeerali et al. 2013), with very few studies conducted in the HF-ISO context. The use of a regional coupled model with the diagnostics presented in this study could provide a way to unravel the complex nonlinear linkage between different space and time scale phenomena in the ISM. However, this warrants an improvement of the model ISO structures, particularly when the ISO modes are undergoing a change in its intensity and variability, and partly in conjunction with increased rainfall extremes (Karmakar et al. 2017a).

Acknowledgements We thank two anonymous reviewers for their constructive comments and suggestions. We would like to thank Tracy Ippolito of COAPS, FSU for the editorial assistance in editing an earlier version of this manuscript. This work was funded by NASA Grants NNX17AG72G, NNX16AD83G, NSF award number 1606296 and the Earth System Science Organization, Ministry of Earth Sciences, Government of India (MM/SERP/FSU/2014/SSC-02/002).

References

Allen M, Robertson A (1996) Distinguishing modulated oscillations from coloured noise in multivariate datasets. Clim Dyn 12(11):775–784. https://doi.org/10.1007/s003820050142

Alpert JC, Kanamitsu M, Caplan PM, Sela JG, White G, Kalnay E (1988) Mountain induced gravity wave drag parameterization in the NMC medium-range forecast model. In: Proceedings of 8th conference on numerical weather prediction, American Meteor Society, Baltimore, MD, pp 726–733

Ananthakrishnan R, Acharya U, Ramakrishnan A (1967) On the criteria for declaring the onset of the southwest monsoon over Kerala. Forecasting Manual FMU Report No IV-181, 52, pp 1620–1639

Bansod S, Singh S, Kripalani R (1991) The relationship of monsoon onset with subsequent rainfall over India. Int J Clim 11(7):809–817

Carton JA, Giese BS (2008) A reanalysis of ocean climate using simple ocean data assimilation (SODA). Mon Weather Rev 136(8):2999–3017. https://doi.org/10.1175/2007MWR1978.1

Chen T, Chen J (1993) The 10–20-day mode of the 1979 Indian monsoon: its relation with the time variation of monsoon rainfall. Mon Weather Rev 121:2465–2482. https://doi.org/10.1175/1520-0493(1993)121<2465:TDMOTI>2.0.CO;2

Chou MD, Suarez MJ (1994) An efficient thermal infrared radiation parameterization for use in general circulation models. Tech. rep., NASA Tech. Memo. NASA-TM-104606

Chou M, Lee K, Tsay S, Fu Q (1999) Parameterization for cloud longwave scattering for use in atmospheric models. J Clim 12:159–169. https://doi.org/10.1175/1520-0442-12.1.159

Dee D, Uppala S, Simmons A, Berrisford P, Poli P, Kobayashi S, Andrae U, Balmaseda M, Balsamo G, Bauer P et al (2011) The ERA-Interim reanalysis: configuration and performance of the data assimilation system. Q J R Meteorol Soc 137(656):553–597. https://doi.org/10.1002/qj.828

Ek M, Mitchell K, Lin Y, Rogers E, Grunmann P, Koren V, Gayno G, Tarpley J (2003) Implementation of Noah land surface model advances in the National Centers for Environmental Prediction operational mesoscale Eta model. J Geophys Res Atmos 108:D22

Gadgil S (2003) The Indian monsoon and its variability. Annu Rev Earth Planet Sci 31(1):429–467. https://doi.org/10.1146/annurev.earth.31.100901.141251

Gadgil S, Gadgil S (2006) The Indian monsoon, GDP and agriculture. Econ Polit Wkly 20:4887–4895

Ghil M, Allen M, Dettinger M, Ide K, Kondrashov D, Mann M, Robertson AW, Saunders A, Tian Y, Varadi F et al (2002) Advanced spectral methods for climatic time series. Rev Geophys 40(1):31–341. https://doi.org/10.1029/2000RG000092

Giné X, Townsend RM, Vickery J (2008) Rational expectations? Evidence from planting decisions in semi-arid India. Working paper No 166, World Bank, Washington, DC

Goswami BN, Ajaya Mohan RS (2001) Intraseasonal oscillations and interannual variability of the Indian summer monsoon. J Clim 14:1180–1198. https://doi.org/10.1175/1520-0442(2001)014<1180:IOAIVO>2.0.CO;2

Hong Y, Pan H (1996) Nonlocal boundary layer vertical diffusion in a medium-range forecast model. Mon Weather Rev 124:2322–2339. https://doi.org/10.1175/1520-0493(1996)124<2322:NBLVDI>2.0.CO;2

Huffman GJ, Bolvin DT, Nelkin EJ, Wolff DB, Adler RF, Gu G, Hong Y, Bowman KP, Stocker EF (2007) The TRMM multisatellite precipitation analysis (TMPA): Quasi-global, multiyear, combined-sensor precipitation estimates at fine scales. J Hydrometeorol 8(1):38–55. https://doi.org/10.1175/JHM560.1

Joseph PV, Eischeid JK, Pyle RJ (1994) Interannual variability of the onset of the Indian summer monsoon and its association with atmospheric features, El Nino, and sea surface temperature anomalies. J Clim 7(1):81–105

Joseph PV, Sooraj KP, Rajan CK (2006) The summer monsoon onset process over South Asia and an objective method for the date of monsoon onset over Kerala. Int J Climatol 26(13):1871–1893

Jourdain NC, Gupta AS, Taschetto AS, Ummenhofer CC, Moise AF, Ashok K (2013) The Indo-Australian monsoon and its relationship to ENSO and IOD in reanalysis data and the CMIP3/CMIP5 simulations. Clim Dyn 41(11–12):3073–3102

Juang HMH, Kanamitsu M (1994) The nmc nested regional spectral model. Mon Weather Rev 122(1):3–26

Kanamitsu M, Ebisuzaki W, Woollen J, Yang SK, Hnilo J, Fiorino M, Potter G (2002) NCEP-DOE AMIP-II Reanalysis (R-2). Bull Am Meteorol Soc 83(11):1631–1644. https://doi.org/10.1175/BAMS-83-11-1631

Kanamitsu M, Yoshimura K, Yhang YB, Hong SY (2010) Errors of interannual variability and trend in dynamical downscaling of reanalysis. J Geophys Res Atmos 115:D17

Karmakar N, Krishnamurti TN (2018) Characteristics of northward propagating intraseasonal oscillation in the Indian summer monsoon. Clim Dyn. https://doi.org/10.1007/s00382-018-4268-2

Karmakar N, Misra V (2019) The relation of intraseasonal variations with local onset and demise of the indian summer monsoon. J Geophys Res-Atmos 124(5):2483–2506

Karmakar N, Chakraborty A, Nanjundiah RS (2017a) Increased sporadic extremes decrease the intraseasonal variability in the Indian summer monsoon rainfall. Sci Rep 7:7824. https://doi.org/10.1038/s41598-017-07529-6

Karmakar N, Chakraborty A, Nanjundiah RS (2017b) Space-time evolution of the low- and high-frequency intraseasonal modes of the Indian Summer Monsoon. Mon Weather Rev 145(2):413–435. https://doi.org/10.1175/MWR-D-16-0075.1

Krishnamurthy V, Shukla J (2007) Intraseasonal and seasonally persisting patterns of Indian monsoon rainfall. J Clim 20(1):3–20. https://doi.org/10.1175/JCLI3981.1

Krishnamurti TN, Bhalme HN (1976) Oscillations of a monsoon system. Part I. Observational aspects. J Atmos Sci 33:1937–1954. https://doi.org/10.1175/1520-0469(1976)033<1937:OOAMSP>2.0.CO;2

Krishnamurti TN, Ramanathan Y (1982) Sensitivity of the monsoon onset to differential heating. J Atmos Sci 39(6):1290–1306

Krishnamurti TN, Jayakumar PK, Sheng J, Surgi N, Kumar A (1985) Divergent circulations on the 30 to 50 day time scale. J Atmos Sci 42:364–375. https://doi.org/10.1175/1520-0469(1985)042<0364:DCOTTD>2.0.CO;2

Krishnamurti TN, Simon A, Thomas A, Mishra A, Sikka D, Niyogi D, Chakraborty A, Li L (2012) Modeling of forecast sensitivity on the march of monsoon isochrones from Kerala to New Delhi: the first 25 days. J Atmos Sci 69(8):2465–2487

Large WG, McWilliams JC, Doney SC (1994) Oceanic vertical mixing: a review and a model with a nonlocal boundary layer parameterization. Rev Geophys 32(4):363–403

Lau K, Yang S (1996) Seasonal variation, abrupt transition, and intraseasonal variability associated with the Asian summer monsoon in the GLA GCM. J Clim 9(5):965–985

Lee JY, Wang B, Wheeler MC, Fu X, Waliser DE, Kang IS (2013) Real-time multivariate indices for the boreal summer intraseasonal oscillation over the Asian summer monsoon region. Clim Dyn 40(1–2):493–509

Li H, Misra V (2014) Thirty-two-year ocean-atmosphere coupled downscaling of global reanalysis over the intra-american seas. Clim Dyn 43(9):2471–2489. https://doi.org/10.1007/s00382-014-2069-9

Lin JL, Weickman KM, Kiladis GN, Mapes BE, Schubert SD, Suarez MJ, Bacmeister JT, Lee MI (2008) Subseasonal variability associated with Asian summer monsoon simulated by 14 IPCC AR4 coupled GCMs. J Clim 21(18):4541–4567

Mellor GL, Yamada T (1982) Development of a turbulence closure model for geophysical fluid problems. Rev Geophys 20(4):851–875

Misra V, Bhardwaj A, Mishra A (2017a) Local onset and demise of the Indian summer monsoon. Clim Dyn. https://doi.org/10.1007/s00382-017-3924-2

Misra V, Bhardwaj A, Noska R (2017b) Understanding the variations of the length and the seasonal rainfall anomalies of the Indian Summer Monsoon. J Clim 30(5):1753–1763

Misra V, Mishra A, Bhardwaj A (2017c) High-resolution regional-coupled ocean-atmosphere simulation of the indian summer monsoon. Int J Climatol 37(S1):717–740

Misra V, Mishra A, Bhardwaj A (2018) Simulation of the intraseasonal variations of the indian summer monsoon in a regional coupled ocean-atmosphere model. J Clim 31(8):3167–3185. https://doi.org/10.1175/JCLI-D-17-0434.1

Moorthi S, Suarez MJ (1992) Relaxed arakawa-schubert. A parameterization of moist convection for general circulation models. Mon Weather Rev 120(6):978–1002. https://doi.org/10.1175/1520-0493(1992)120<0978:RASAPO>2.0.CO;2

Moron V, Robertson AW (2014) Interannual variability of Indian summer monsoon rainfall onset date at local scale. Int J Clim 34(4):1050–1061

Moron V, Robertson A, Ghil M (2012) Impact of the modulated annual cycle and intraseasonal oscillation on daily-to-interannual rainfall variability across monsoonal India. Clim Dyn 38(11–12):2409–2435. https://doi.org/10.1007/s00382-011-1253-4

Noska R, Misra V (2016) Characterizing the onset and demise of the Indian summer monsoon. Geophys Res Lett 43(9):4547–4554

Pai DS, Sridhar L, Rajeevan M, Sreejith O, Satbhai N, Mukhopadhyay B (2014) Development of a new high spatial resolution (0.25× 0.25) long period (1901–2010) daily gridded rainfall data set over India and its comparison with existing data sets over the region. Mausam 65(1):1–18

Pegion K, Kirtman BP (2008) The impact of air–sea interactions on the simulation of tropical intraseasonal variability. J Clim 21(24):6616–6635

Plaut G, Vautard R (1994) Spells of low-frequency oscillations and weather regimes in the Northern Hemisphere. J Atmos Sci 51(2):210–236. https://doi.org/10.1175/1520-0469(1994)051

Rajeevan M, Unnikrishnan C, Bhate J, Niranjan Kumar K, Sreekala P (2012) Northeast monsoon over India: variability and prediction. Meteorol Appl 19(2):226–236

Rajendran K, Kitoh A, Mizuta R, Sajani S, Nakazawa T (2008) High-resolution simulation of mean convection and its intraseasonal variability over the tropics in the MRI/JMA 20-km mesh AGCM. J Clim 21(15):3722–3739

Sabeerali C, Ramu Dandi A, Dhakate A, Salunke K, Mahapatra S, Rao SA (2013) Simulation of boreal summer intraseasonal oscillations in the latest CMIP5 coupled GCMs. J Geophys Res-Atmos 118(10):4401–4420

Sharmila S, Pillai P, Joseph S, Roxy M, Krishna R, Chattopadhyay R, Abhilash S, Sahai A, Goswami B (2013) Role of ocean–atmosphere interaction on northward propagation of Indian summer monsoon intra-seasonal oscillations (MISO). Clim Dyn 41(5–6):1651–1669

Shchepetkin AF, McWilliams JC (2005) The regional oceanic modeling system (ROMS): a split-explicit, free-surface, topography-following-coordinate oceanic model. Ocean Model 9(4):347–404

Sikka D, Gadgil S (1980) On the maximum cloud zone and the ITCZ over Indian, longitudes during the southwest monsoon. Mon Weather Rev 108(11):1840–1853. https://doi.org/10.1175/1520-0493(1980)108<1840:OTMCZA>2.0.CO;2

Sperber KR, Annamalai H (2008) Coupled model simulations of boreal summer intraseasonal (30–50 day) variability, Part 1: Systematic errors and caution on use of metrics. Clim Dyn 31(2–3):345–372

Sperber KR, Annamalai H (2014) The use of fractional accumulated precipitation for the evaluation of the annual cycle of monsoons. Clim Dyn 43(12):3219–3244

Tiedtke M (1983) The sensitivity of the time-mean large-scale flow to cumulus convection in the ECMWF model. In: Workshop on convection in large-scale numerical models, 28 November to 1 December 1983. ECMWF, ECMWF, Shinfield Park, Reading, pp 297–316

Umlauf L, Burchard H (2003) A generic length-scale equation for geophysical turbulence models. J Mar Res 61(2):235–265

Waliser D, Jin K, Kang IS, Stern W, Schubert S, Wu M, Lau KM, Lee MI, Krishnamurthy V, Kitoh A et al (2003) AGCM simulations of intraseasonal variability associated with the Asian summer monsoon. Clim Dyn 21(5–6):423–446

Wang B, Lin H (2002) Rainy season of the Asian-Pacific Summer Monsoon. J Clim 15(4):386–398. https://doi.org/10.1175/1520-0442(2002)015<0386:RSOTAP>2.0.CO;2

Wang B, Ding Q, Joseph PV (2009a) Objective definition of the Indian summer monsoon onset. J Clim 22(12):3303–3316

Wang W, Chen M, Kumar A (2009b) Impacts of ocean surface on the northward propagation of the boreal summer intraseasonal oscillation in the NCEP climate forecast system. J Clim 22(24):6561–6576

Webster PJ, Yang S (1992) Monsoon and ENSO: selectively interactive systems. Q J R Meteorol Soc 118(507):877–926

Webster PJ, Magaña VO, Palmer TN, Shukla J, Tomas RA, Yanai M, Yasunari T (1998) Monsoons: processes, predictability, and the prospects for prediction. J Geophys Res-Oceans 103(C7):14,451–14,510. https://doi.org/10.1029/97JC02719

Yanai M, Li C, Song Z (1992) Seasonal heating of the Tibetan Plateau and its effects on the evolution of the Asian summer monsoon. J Meteor Soc Jpn Ser II 70(1B):319–351

Yasunari T (1980) A quasi-stationary appearance of 30 to 40 day period in the cloudiness fluctuations during the summer monsoon over India. J Meteor Soc Jpn 58:225–229

Zhao Q, Carr FH (1997) A prognostic cloud scheme for operational NWP models. Mon Weather Rev 125(8):1931–1953. https://doi.org/10.1175/1520-0493(1997)125<1931:APCSFO>2.0.CO;2

Zhou L, Murtugudde R (2014) Impact of northward-propagating intraseasonal variability on the onset of Indian summer monsoon. J Clim 27(1):126–139